Journal of Solid State Chemistry **158,** 268–278 (2001)
doi:10.1006/jssc.2001.9107, available online at http://www.idealibrary.com on IDEAL®

The Mechanisms of Combustion and Continuous Reactions during Mechanical Alloying

N. J. Calos,* J. S. Forrester,†,[1] and G. B. Schaffer‡

*Department of Chemistry and Department of Earth Sciences, The University of Queensland, Queensland 4072, Australia; †Department of Mechanical Engineering, University of Newcastle, Callaghan, New South Wales 2308, Australia; and ‡Department of Mining, Minerals and Materials Engineering, The University of Queensland, Queensland 4072, Australia

Received October 13, 2000; in revised form December 14, 2000; accepted January 19, 2001; published online April 5, 2001

Some materials exhibit a combustion event during mechanical alloying, which results in the rapid transformation of reactants into products, while others show a slow transformation of reactants into products. In this paper, the continuous W + C → WC reaction is compared to the Ti + C → TiC combustion reaction. Rietveld refinement of X-ray diffraction patterns is used to show that these particular reactions proceed through different pathways, determined by crystallographic factors of the reactants. When a crystallographic relationship exists between the reactants and the products, such as that between W and WC, the product forms slowly over a period of time. In contrast, insertion of C into the Ti structure is associated with atomic rearrangements within the crowded lattice planes and the subsequent catastrophic failure of the reactant lattices results in combustion to form TiC. © 2001 Academic Press

INTRODUCTION

Mechanical alloying (MA) is a powder metallurgy technique that involves the mechanical milling of reactants to form product phases. MA has been used for many years as a method of producing novel materials (1–3); however, there are many aspects of MA that have not yet been explained. For example, it has been shown that the alloying of some precursor materials results in a violent combustion reaction in which there is an instant alteration of reactions to products. Other materials show a continuous transformation over a period of time (4, 5). The current work examines why some systems combust, while other nominally similar systems do not.

Two similar systems were to be examined, and a recent study of carbides (6) suggested that these systems were suitable. Some carbides that form during MA do so by combustion and others by a continuous reaction. Le Caër *et al.* (6) demonstrated that many carbides and silicides could be synthesised by the MA of elemental powders, producing both stable and metastable compounds with a high defect density. Some of these materials were found to be partially reacted following 24 h of milling, while others were totally transformed into the reacted product.

Cottrell (7) suggested that the possible crystallographic locations of carbon atoms in the unit cell determine if a carbide can form and that the crystal structure of the carbide depends on the nearest neighbors of the carbon atoms and whether the carbon atoms are in octahedral or trigonal configurations. This has been used to explain the formation of many transition metal carbides, including simple formations, such as TiC, and the complicated Mn and C formations, such as $Mn_{23}C_6$.

The aim of the research presented here is to develop the notion that the formation of carbides during mechanical alloying is also controlled by crystallographic constraints.

EXPERIMENTAL

Materials were prepared using mechanical alloying procedures as outlined in Forrester and Schaffer (8). Stoichiometric quantities of W, Ti, and C were prepared to form the products WC and TiC. The charge ratio (CR) was 30:1 and yttria tetragonal zirconia (YTZ) balls were used as the grinding media. These were sealed in a hardened steel vial under an argon atmosphere and milled in a SPEX 8000 mixer/mill. W and C were milled for 10 min, 1 h, 2 h, 4 h, 10 h, and 24 h. Ti and C were milled for 10, 20, 30, and 33 min (the final milling time was postcombustion). Materials were then quenched in liquid nitrogen to prevent further diffusion of reactant atoms from occurring (aging of materials in MA is known to promote further reaction (9)).

X-ray diffraction (XRD) patterns of the materials were collected using a Philips PW1130 diffractometer using Cu$K\alpha$ radiation. Rietveld analysis was performed on the patterns using the Rietveld refinement computer program

[1] To whom correspondence should be addressed.

0022-4596/01 $35.00

LHPM8 (10, 11). Anisotropic Gaussian atomic displacement parameters (ADPs) from these analyses were used in the computer program ATOMS V3.1 (Shape Software, E. Dowty © 1995) in order to visualize the thermal ellipsoids and study the reaction pathway.

RESULTS

Initial crystal structures for reactants and products were obtained from the JCPDS database (12). The crystal structure of W is cubic with space group $Im3m$, and unit cell, $a_0 = 3.1648$ Å. The crystal structure of graphite is hexagonal, $P6_3/mmc$, with unit cell $a_0 = 2.4704$ Å, $c_0 = 6.7244$ Å. The product phase WC is also hexagonal, has a space group $P\text{-}6m2$ and a unit cell, $a_0 = 2.9034$ Å, $c_0 = 2.8416$ Å. The crystal structure of Ti is hexagonal, with space group $P6_3/mmc$ and a unit cell $a_0 = 2.9538$ Å, $c_0 = 4.6881$ Å. The product phase of TiC is cubic, $Fm3m$, $a_0 = 4.3274$ Å.

XRD patterns of the processed materials are shown in Figs. 1 and 2. The formation of WC through the milling of W and C is shown in Figs. 1a and 1b. After milling for 10 min C has become undetectable by XRD. The W peaks have broadened significantly. After 1 h of milling, the intermediate phase W_2C and the product WC are observable in small proportions. The proportion of W decreases as milling progresses and is in rapid decline after 10 h of milling. The proportions of W_2C and WC increase, but after 10 h of milling W_2C also declines, and at 24 h, the XRD pattern shows only WC present.

In contrast, XRD patterns of Ti and C through milling to combustion are shown in Fig. 2. Although the Ti diffraction peaks broaden during milling, they remain relatively unchanged through 30 min of milling. Intermediate phases do not occur. The major C diffraction peak ($\sim 26^\circ$ 2θ) undergoes significant broadening, but remains visible after 30 min of milling. Between 30 and 33 min there is a rapid alteration of the reactants to the product TiC.

Rietveld analysis of the XRD patterns allows the reactions to be examined in greater detail. The refinement of W and C milled 4 h is shown in Fig. 3, with the phases detectable being W, W_2C, and WC. The Ti and C refinement after 10 min of milling is shown in Fig. 4, showing only elemental powders present. All major diffraction intensity is accounted for by the calculated patterns in both refinements, although peak broadening has produced an inferior fit in the W and C refinement. The Bragg R factors for these refinements are 6.56 and 1.53, respectively. The Rietveld refinement parameters for W and C are shown in Tables 1–9 and those of Ti and C are shown in Tables 10–13.

Information on crystallite size and strain may also be retrieved from the diffraction peak shapes in the course of Rietveld analysis (14). Therefore, one noteworthy feature in Tables 1, 2, 3, and 8 is the change in the u term of the Bragg peak Gaussian components. This is related to the accumu-

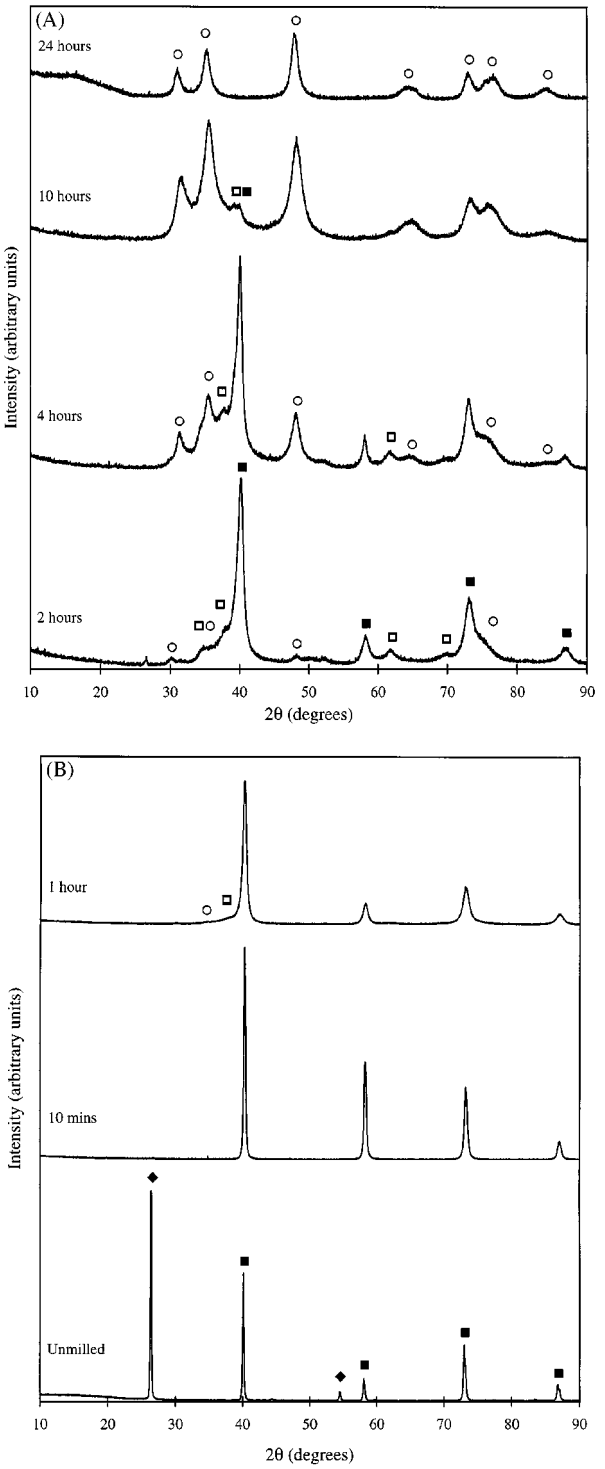

FIG. 1. (A) Milling of W and C from unmilled to 1 h using YTZ grinding balls with CR30 : 1. There is broadening of the W peaks after 10 min, and after 1 h W_2C and WC intermediate and product phases appear. (◆) C, (■) W, (□) W_2C, (○) WC. (B) Milling of W and C from 2 to 24 h. As milling progresses, the precursor W and C diffraction peaks are gradually replaced by W_2C and WC peaks. With 24 h of milling, WC is the only phase clearly visible in the diffraction pattern. (■) W, (□) W_2C, (○) WC.

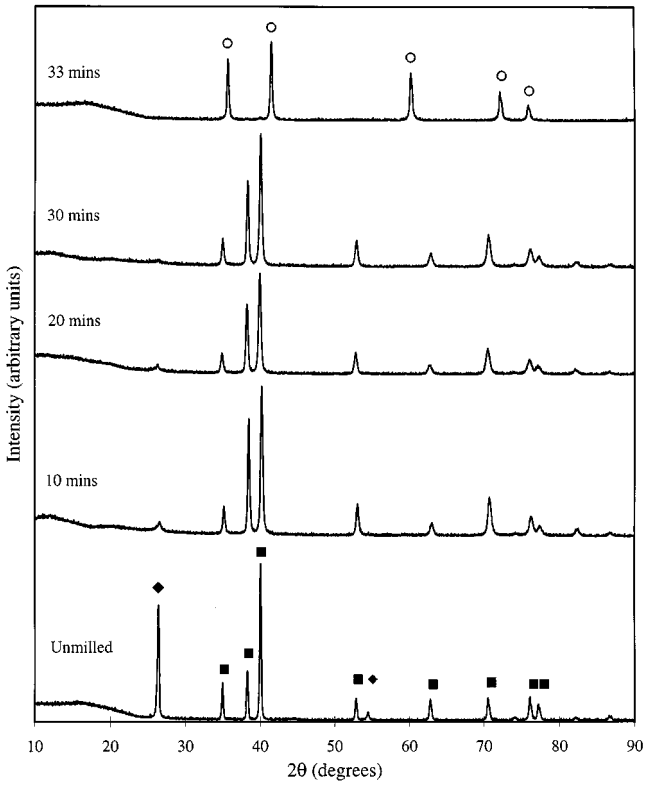

FIG. 2. XRD patterns of Ti and C unmilled and milled for 10, 20, 30, and 33 min. There is little peak broadening in the Ti diffraction peaks, whereas C broadens soon after milling commences. (◆) C, (■) Ti, (○) TiC.

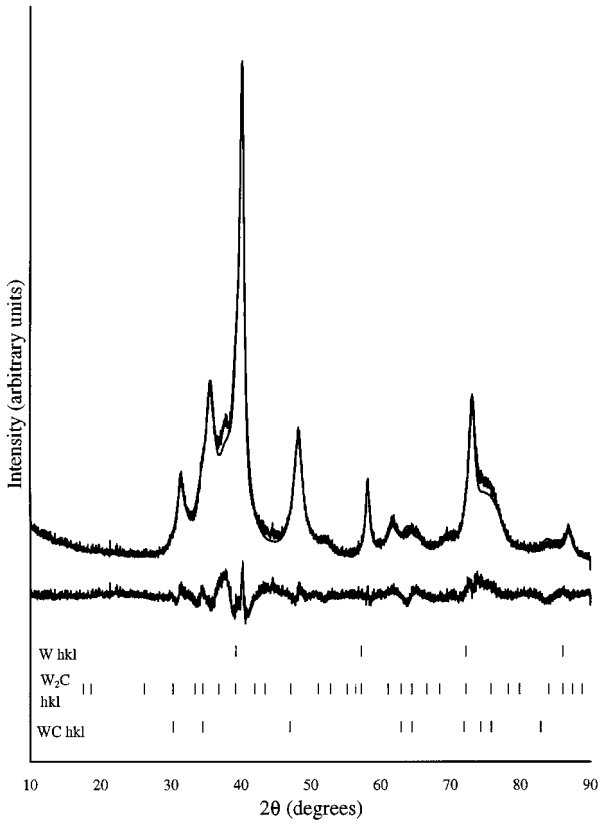

FIG. 3. Rietveld refinement of W and C milled for 4 h. The experimental trace and the calculated pattern are overlayed, with the difference pattern below. The markers beneath are the *hkl* markers for each of the phases.

lated strain in the materials. The *u* term for W (Table 1) increases until 1 h of milling and thereafter decreases. The strain parameters for W_2C (Table 3) are initially high and decrease with greater milling times. The strain parameter for WC (Table 8) is high until WC is fully formed (at 24 h).

The refinements of Ti and C with increasing milling times show an increase in the *u* term (Tables 10 and 12). Although there is some increase in the *u* term of Ti as milling progresses (from 0.0897 to 0.3392), indicating some strain accumulation in Ti. Increases in the *u* term in C are large. This is clear evidence of strain accumulation in the C. Moderate peak broadening of the Ti reflections and extensive broadening of the major C reflection in the XRD patterns (Fig. 2) also supports this finding.

Tables 4–7 show the anisotropic Gaussian displacement parameters (ADPs) of refined W_2C from 1 to 10 h milling time. Table 9 contains the ADPs for WC (15). The ADPs during WC formation are examined visually in Fig. 5. In all cases, the smaller ellipsoids represent W atoms. Figures 5a and 5b show the 95% probability ellipsoids of W and C atoms in the WC phase which is forming after 1 h of milling. The small ellipsoids represent the statistically occupied areas where W atoms may be found with 95% probability, and the large ellipsoids are those statistically occupied by C atoms.

Figures 5c and 5d show the 95% probability ellipsoids of the atoms of the WC phase at 24 h of milling. The volume occupied by the W and C atoms becomes more defined here than in the initial state. Figures 5e and 5f are the probability ellipsoids for W_2C when the material has been milled for 2 h. The elongation of the carbon ellipsoids indicates easy atomic movement along the *c* axis in W_2C.

Tables 11 and 13 present the ADPs of Ti and C. The ADPs of Ti remain unchanged as milling progresses, and those of C show an increase, but not to the scale of W and C. The easy atomic motion of W and C shown in Fig. 5 has clearly not occurred in the Ti/C system.

Anisotropic strains occurring in titanium prior to combustion were assessed by comparison of the peaks representing high symmetry planes against the "whole pattern" expectation widths. Individual peaks were fitted using the formula given by Caglioti *et al.* (16) for isotropic diffraction peak broadening effects. This comparison is shown in Table 14 and in Fig. 6.

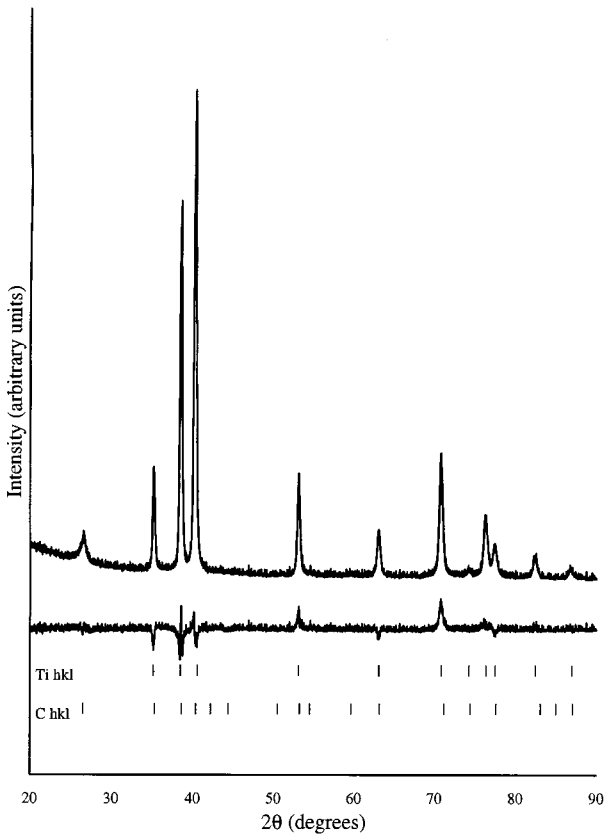

FIG. 4. Rietveld refinement of Ti and C milled for 10 min. The experimental trace and the calculated pattern are overlayed, with the difference pattern below. The markers beneath are the *hkl* markers for each of the phases.

DISCUSSION

It has been established that it is possible to trace the pathway of a chemical reaction using ADPs (17, 18). Here, this visualization is used to compare the crystallographic relationships between the formation of WC and TiC and the occurrence or absence of a combustion reaction.

TABLE 1
Rietveld Refinement Parameters for W

Milling time	u	w	Lorentzian	W unit cell a (Å)	β_{11}[a] (Å^2)	Bragg R factor
0 min	0.083	0.015	0.544	3.168	0.0004	17.2
10 min	0.343	0.018	0.521	3.170	0.0008	28.7
1 h	1.436	0.198	0.855	3.163	0.0009	2.6
2 h	1.233	0.850	1.069	3.164	0.0008	4.3
4 h	1.111	0.284	1.067	3.167	0.0011	2.7
10 h	0.269	0.629	1.888	3.151	0.0015	3.4

[a] $\beta_{11} = \beta_{22} = \beta_{33}$, and $\beta_{12} = \beta_{13} = \beta_{23} = 0$ by symmetry (13).

TABLE 2
Rietveld Refinement Parameters for C

Milling time (min)	u	w	Lorentzian	C unit cell (Å) a	C unit cell (Å) c	B_{iso} (Å^2)	Bragg R factor
0	0.174	0.002	0.497	N/A	6.721	0.1706	2.6
10	0.929	0.518	1.553	2.478	6.778	1	13.8

The Continuous Reaction (W/C)

The reaction of W and C to form WC is a continuous process passing through a disordered W_2C phase. This is in contrast to the findings of Wang *et al.* (19), who indicate that the formation of W and C to form WC passes through no intermediate phases. The intermediate phase W_2C is easily overlooked due to the broadness of diffraction intensity produced by MA XRD patterns.

Milling of W produces strains and lattice defects into which C atoms may ingress. The gradual infilling of interstices redefines the bond schemes and allows resultant shear planes to restructure the lattice as carbide-type. Insertion of C into tetrahedral vacancies in the W lattice facilitates parting of the most densely packed and widely separated planes for BCC, i.e., the $\{1\,1\,0\}$ slip planes with associated lattice strain (20). It is worth noting here for later comparison with the close-packed Ti that although interstices in the BCC structure are relatively smaller than in HCP or FCC, the actual free volume of the W lattice is much larger. This means there is less resistance to matrix rearrangement than in Ti.

XRD patterns (Fig. 1) show the transformation of W into W_2C and then into WC. The development of the W_2C (0 0 2) peak from the W (1 1 0) peak and the subsequent development of the WC (0 0 1) peak indicate this. As W incorporates C, slippage in the $\{1\,1\,0\}$ planes of the cubic cell allow redefinition of the W sublattice to that of the W_2C lattice. In

TABLE 3
Rietveld Refinement Parameters for W_2C

Milling time (h)	u	w	Lorentzian	W_2C unit cell (Å) a	W_2C unit cell (Å) c	Bragg R factor
1	4.801	1.583	1.109	5.162	4.739	2.2
2	2.008	2.441	− 0.045	5.164	4.748	3.7
4	0.098	3.887	1.363	5.201	4.753	2.1
10	0.162	3.658	1.846	5.192	4.753	2.5

TABLE 4
Anisotropic Displacement Parameters for W_2C Milled 1 h

Atom	Anisotropic displacement parameters					
	β_{11}(Å^2)	β_{22}(Å^2)	β_{33}(Å^2)	β_{12}(Å^2)	$\beta_{13}{}^a$(Å^2)	$\beta_{23}{}^a$(Å^2)
W	0.0018	0.0525	0.0259	0.0263	0.0185	—
C	0.0002	0.0002	0.0574	0.0001	—	—
C	0.0002	0.0002	0.0574	0.0001	—	—
C	0.0002	0.0002	0.0574	0.0001	—	—

TABLE 6
Anisotropic Displacement Parameters for W_2C Milled 4 h

Atom	Anisotropic displacement parameters					
	β_{11}(Å^2)	β_{22}(Å^2)	β_{33}(Å^2)	β_{12}(Å^2)	$\beta_{13}{}^a$(Å^2)	$\beta_{23}{}^a$(Å^2)
W	0.0619	0.0368	0.0656	0.0184	0.0484	—
C	0.0946	0.0946	5.9100	0.0473	—	—
C	0.0946	0.0946	5.9100	0.0473	—	—
C	0.0946	0.0946	5.9100	0.0473	—	—

the [1 1 1] projection, the ABCA layering transforms to ABAB-type layering. There exists a direct crystallographic relation between W and W_2C:

$$H = \begin{pmatrix} 1 & \bar{1} & 0 \\ 0 & 1 & \bar{1} \\ 1 & 1 & 1 \end{pmatrix} C.$$

This relationship is expressed graphically in Figs. 7 and 8, in which the body diagonal of the cubic cell forms the unique axis of the distorted hexagonal cell.

Previous structures reported for W_2C contain vacancies and statistical occupancy of C sites (21, 22). Therefore, the variable compositions allowed for this structure type are consistent with W_2C being an inclusion/intercalation compound. That is, C interstitially incorporated into the W lattice facilitates $\langle 1\,1\,0 \rangle$ slippage on $\{1\,1\,1\}$. The trigonal projection of the W atoms redefines the hexagonal W_2C lattice.

In the continuing course of the reaction, as more C atoms are included into W_2C, the lattice may be redefined as a trigonal subcell, with roughly 1/6 of the initial volume. In fact, this basal redefinition apparently occurs in the fully ordered W_2C phase, with space group $P6_3/mmc$ and $a_0 = 2.98$ Å, $c_0 = 4.71$ Å (23). The W atoms of W_2C are in the exact geometric arrangement for the WC lattice. The inclusion of extra carbon forces the layers on $\{0\,0\,1\}$ W_2C further apart, with

$$c_0 \text{ WC} \approx c_0 \text{ } W_2C/2,$$

so the transformation matrix between the product and reactant lattices becomes

$$H^1 = \begin{pmatrix} \frac{2}{3} & \frac{1}{3} & 0 \\ \frac{\bar{1}}{3} & \frac{1}{3} & 0 \\ 0 & 0 & \frac{1}{2} \end{pmatrix} H.$$

The 95% probability ellipsoids of the ADPs for W_2C (Figs. 5e and 5f) show the possible diffusion pathway of C atoms along the c axis, while the W atoms move aside (along [1 1 0]). Atomic motion of W along [1 1 0] in the W_2C brings about the collapse of W sites to those of WC. The C atoms (statistically) occupy their mean sites as layers intercalated within the W atomic layers established by C inclusion into W_2C. Atomic arrangements in the starting material are close to the product; i.e. a crystallographic relationship exists between the two.

According to Goldschmidt (24), there exists a link between interstitial compounds and primary solid solutions. Although the interstitial atoms may control these structure transformations, their presence is not an intrinsic condition.

TABLE 5
Anisotropic Displacement Parameters for W_2C Milled 2 h

Atom	Anisotropic displacement parameters					
	β_{11}(Å^2)	β_{22}(Å^2)	β_{33}(Å^2)	β_{12}(Å^2)	$\beta_{13}{}^a$(Å^2)	$\beta_{23}{}^a$(Å^2)
W	0.0208	0.0024	0.0208	0.0012	0.0277	—
C	0.0008	0.0008	0.0759	0.0004	—	—
C	0.0008	0.0008	0.0759	0.0004	—	—
C	0.0008	0.0008	0.0759	0.0004	—	—

TABLE 7
Anisotropic Displacement Parameters for W_2C Milled 10 h

Atom	Anisotropic displacement parameters					
	β_{11}(Å^2)	β_{22}(Å^2)	β_{33}(Å^2)	β_{12}(Å^2)	$\beta_{13}{}^a$(Å^2)	$\beta_{23}{}^a$(Å^2)
W	0.0227	0.0674	0.0411	0.0337	0.0383	—
C	0.2223	0.2223	1.0022	0.1111	—	—
C	0.2223	0.2223	1.0022	0.1111	—	—
C	0.2223	0.2223	1.0022	0.1111	—	—

TABLE 8
Rietveld Refinement Parameters for WC

Milling time (h)	u	w	Lorentzian	WC unit cell (Å) a	WC unit cell (Å) c	Bragg R factor
1	7.292	6.122	0.034	2.849	2.962	2.8
2	2.538	0.698	1.806	2.880	2.875	2.6
4	4.987	1.952	1.120	2.913	2.851	4.3
10	9.033	2.249	1.097	2.938	2.860	2.7
24	0.009	1.305	1.020	2.903	2.842	3.4

TABLE 10
Rietveld Refinement Parameters for Ti

Milling time (min)	u	w	Lorentzian	Ti unit cell (Å) a	Ti unit cell (Å) c	Bragg R factor
0	0.090	0.014	0.560	2.954	4.689	6.9
10	0.300	0.056	0.639	2.953	4.685	6.6
20	0.354	0.076	0.596	2.952	4.682	8.1
30	0.339	0.067	0.625	2.952	4.683	6.9

Interstitial solid solution of C in W is reported for up to 0.3% and at temperatures around 2500°C (25). A comparable example is BCC vanadium → HCP vanadium through the presence of trace N (26–29). That is to say that it is not V_2N that forms, but a structural change in the matrix lattice is stimulated by a few interstitial atoms. The nitridation of V occurs sequentially through tetragonally distorted native metal with interstitial N, to defect trigonal then hexagonal V_2N_{1-x} then to defect VN_{1-x} and finally, NaCl structure type VN. The sequence, constructed from phases identified in the literature is as follows:

$$\underset{Im3m}{V(26)} \rightarrow \underset{I4/mmm}{V_2N_{0.4}(27)} \rightarrow \underset{P\text{-}31m}{V_2N_{0.9}(28)} \rightarrow \underset{P\text{-}31m}{V_2N(28)} \rightarrow \underset{Fm3m}{VN_{0.71}(29)} \rightarrow \underset{Fm3m}{VN(29)}$$

In the V–N series, the intermediate tetragonally distorted lattice has been identified as a separate phase, serving as a case study for the metastable tetragonal W with interstitial C in the 10-min milled experiment (see Fig. 9, below). In addition, Hahn (29) found that the N is able to form superstructural phases in which ordering of the interstitials and vacancies occurs. Such ordering is usually a step toward crystallographic reorientation for formation of the next stable phase.

The shapes of the ADPs (Fig. 5) indicate the reaction pathway for the formation of WC. With the formation of W_2C *en route* from W, there is disorder in the C positions along the crystallographic c-axis of W_2C. There is also attendant disorder in the W positions in the a, b plane as the atoms which move aside from the carbon atom ingress into the metal lattice. The a, b plane disorder is concordant with the $\langle 1\,1\,0 \rangle$ slippage of W in the BCC cubic system. Further in the course of reaction, the ADP ellipsoids of both W and C become more isotropic, as these atoms "settle in" to ordered positions of the product lattice.

Rietveld analysis may be used to examine asymmetry in peak shape due to distortions of the lattice (e.g., (30)). In this case there is notable asymmetry in the (2 0 0) diffraction of W after 10 min of milling (Fig. 9). This particular reflection is sensitive to any tetragonal distortion to the cubic lattice brought about by any inclusion of atoms at interstitial sites. As in martensite, elongation or contraction of one particular axis relative to the others gives a tetragonal unit cell with

TABLE 9
Anisotropic Displacement Parameters for WC

Atom	Anisotropic displacement parameters β_{11}(Å^2)	β_{22}(Å^2)	β_{33}(Å^2)	β_{12}(Å^2)	β_{13}[a](Å^2)	β_{23}[a](Å^2)
W 1 h	0.0096	0.0096	0.0003	0.048	—	—
C 1 h	0.7615	0.7615	0.0029	0.3838	—	—
W 2 h	0.0009	0.0009	0.0008	0.0005	—	—
C 2 h	1.7229	1.7229	0.1178	0.8615	—	—
W 4 h	0.0049	0.0049	0.0012	0.0025	—	—
C 4 h	0.9877	0.9877	0.0007	0.4939	—	—
W 10 h	0.013	0.013	0.0009	0.0065	—	—
C 10 h	1.5525	1.5525	0.0003	0.7763	—	—
W 24 h	0.0018	0.0018	0.0002	0.0009	—	—
C 24 h	0.3319	0.3319	0.0042	0.166	—	—

[a] For atoms on these sites, crystallographic restraints confine these ADPs to zeros (13).

TABLE 11
Anisotropic Displacement Parameters for Ti

Ti	Anisotropic displacement parameters β_{11}(Å^2)	β_{22}(Å^2)	β_{33}(Å^2)	β_{12}(Å^2)	β_{13}[a](Å^2)	β_{23}[a](Å^2)
0 min	0.0002	0.0002	0.0118	0.0001	—	—
10 min	0.0013	0.0013	0.0016	0.0006	—	—
20 min	0.0011	0.0011	0.0017	0.0005	—	—
30 min	0.0011	0.0011	0.0013	0.0005	—	—

[a] For atoms on these sites, crystallographic restraints confine these ADPs to zeros (13).

TABLE 12
Rietveld Refinement Parameters for C

Milling time (min)	u	w	Lorentzian	C unit cell (Å) a	C unit cell (Å) c	Bragg R factor
0	0.260	0.009	0.517	N/A	6.727	1.5
10	9.691	−0.220	1.328	2.483	6.759	1.5
20	11.398	−0.298	1.186	2.481	6.734	2.0
30	13.511	−0.221	1.738	2.475	6.765	1.7

inequivalent $\{h\,0\,0\}$ and $\{0\,0\,h\}$ reflections. In order to analyze the distortions in the W structure after short milling times, a maximal subgroup of $Im3m$ was generated by removal of the three-fold symmetry on [1 1 1] cube, giving $I4/mmm$. The (200) reflection is shown in Fig. 9.

The mechanism for W_2C formation proposed above through a set of W (112) or W ($\bar{1}10$) rearrangements is supported by the low-energy electron diffraction (LEED) study reported by Rawlings *et al.* (31). Their surface analyses of the carburization of single-crystal tungsten (1 1 0) faces show large W_2C-related superstructures coherent with the host lattice. These superstructures, which demonstrate the same orientation relationships as in Figs. 6 and 7, require small periodic displacements of tungsten atoms in the planes of lowest density to form the necessary coincidences of W with W_2C. Therefore, in tungsten, the combination of only minor atomic displacements and low spatial restriction for these arrangements greatly facilitates a smooth transformation of the carbide.

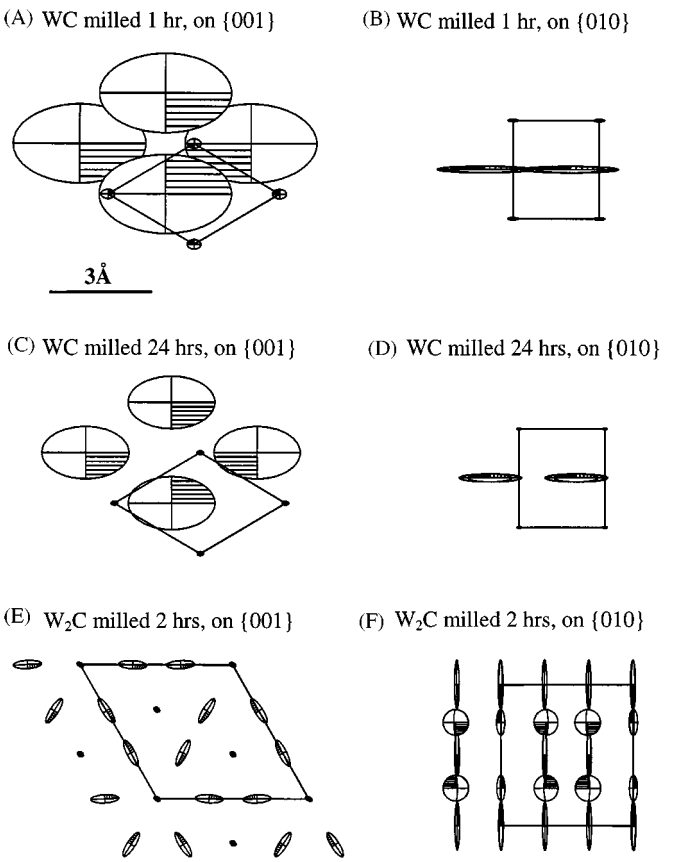

FIG. 5. Crystal structure projections of W and C showing site occupations at 95% probability levels (14). In all cases, W ellipsoids are the smaller ones.

The Combustion Reaction (Ti/C)

As stated by Goldschmidt (24), the transformation of Ti to TiC (HCP to FCC) mirrors the temperature/pressure dependent β-Ti to α-Ti transformation sequence. In this sequence the HCP stage of the W–W_2C–WC sequence is transposed onto the initial stage, rather than the intermediate. That is to say that the initial state of the Ti–C system has some measure of stability, which must be overcome for the reaction to proceed. The primary α-(Ti,C) solid solution evolves from a pseudocompound.

In the Ti–C system, as in the case of the mechanically induced reduction of CuO by Fe, it appears that a critical level of lattice strain and opening of diffusion paths within the Ti lattice induce the reaction. Beyond this critical point, a concerted breaking or unzipping of the basal Ti–Ti bonds and insertion of carbon supplied the additional energy required for a runaway reaction, and combustion occurs.

Although the apparent geometric relationships between reactant and product unit cells suggest a simple layer slip from *ABCABC* to *ABABAB*, the atomic transformations required for the reaction are much more complex. A (111) layer slip entails insertion of foreign atoms into the host HCP lattice in the (110) surface, with alternate columns of matrix atoms forced apart along ($1\bar{1}0$). In contrast to the W_2C formation mechanism, this reaction requires atomic arrangements within close-packed planes.

TABLE 13
Anisotropic Displacement Parameters for C

C	Anisotropic displacement parameters β_{11}(Å^2)	β_{22}(Å^2)	β_{33}(Å^2)	β_{12}(Å^2)	β_{13}[a](Å^2)	β_{23}[a](Å^2)
0 min	$B_{iso}=0.647$	—	—	—	—	—
10 min	0.0531	0.0531	0.0059	0.02653	—	—
20 min	0.0691	0.0691	0.0306	0.0345	—	—
30 min	0.1483	0.1483	0.04345	0.0741	—	—

[a] For atoms on these sites, crystallographic restraints confine these ADPs to zero (13).

TABLE 14
FWHM of Reflexes from Principle Symmetry Planes of Ti

	0 min		30 min	
h k l	Caglioti[a]	Observed	Caglioti[a]	Observed
1 0 0	0.234	0.246	0.322	0.345
0 0 2	0.245	0.26	0.347	0.304[b]
1 0 0	0.349	0.348	0.548	0.573

[a] Expectation peak widths from the formula of Caglioti *et al.* (16).
[b] Asymmetric to high 2θ side of peak.

A model for the reaction of Ti and C may be found in the oxidation of cobalt. The mechanism of transformation of HCP Co (space group $P6_3/mmc$) to *fcc* CoO (space group $Fm3m$) is well established through extensive surface chemistry studies of single crystals. In particular, the LEED analyses of structural changes occurring on (110) and (001) faces of a single crystal, defect-free cobalt during oxygen incorporation provide valuable clues to the pathway by which carbon may incorporate into the titanium lattice (32). To form the new cobalt structure, oxygen must insert on or through the Co (001) face, which will cause considerable in-plane dilation (33). This dilation is also observed in LEED patterns of oxygen penetration of Co (110) faces (34). Thus, an initial onset period is noted with oxygen monolayer formation and oxygen penetration to the subsurface. This is followed by rapid reaction in the subsurface

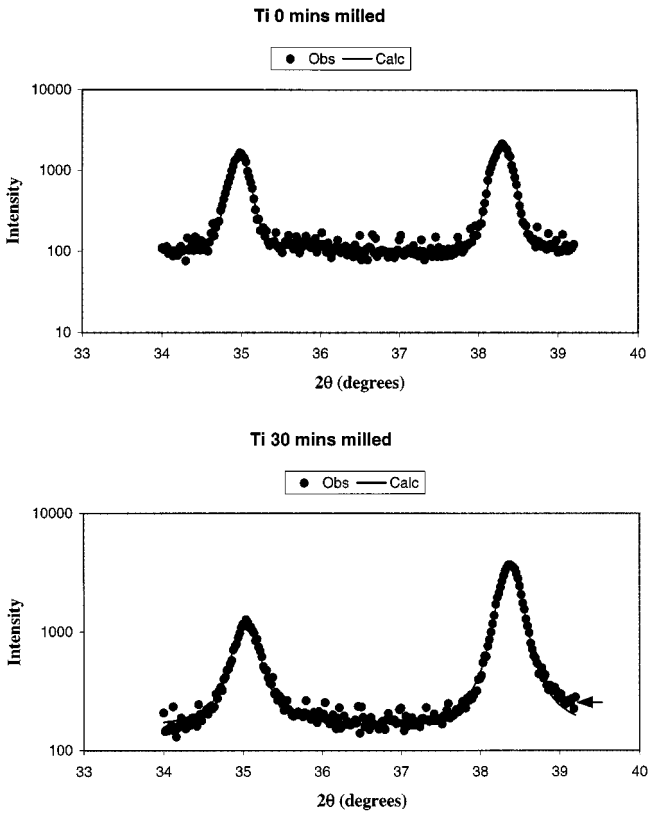

FIG. 6. Comparison of expected peak widths (16) to observed peak widths in 0 min milled and 30 min milled diffraction peaks of Ti. Arrow indicates the high 2θ tail on the (002) diffraction arising from anisotropic broadening of the reciprocal lattice point.

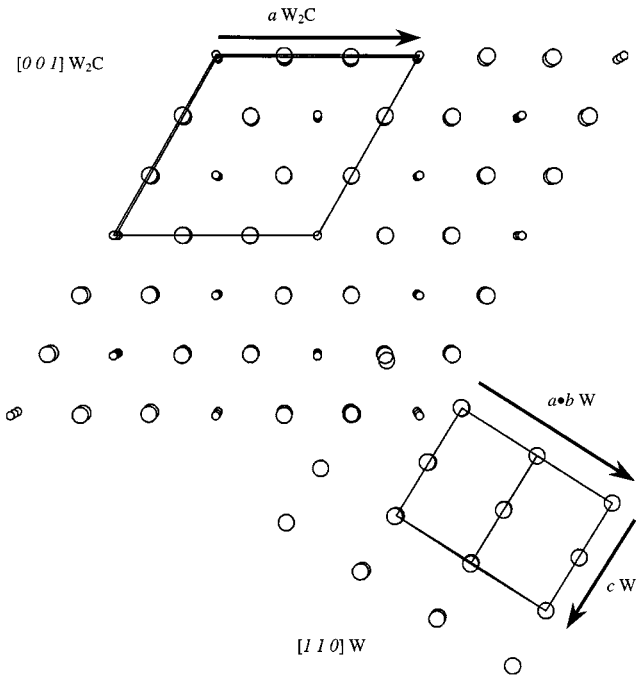

FIG. 7. Crystal structures of W and W_2C showing the crystallographic relationship which exists between the two: superposition of the [1 1 0] W and [0 0 1] W_2C. The solid lines enclose one unit cell of each phase, and large and small circles represent W and C atoms, respectively.

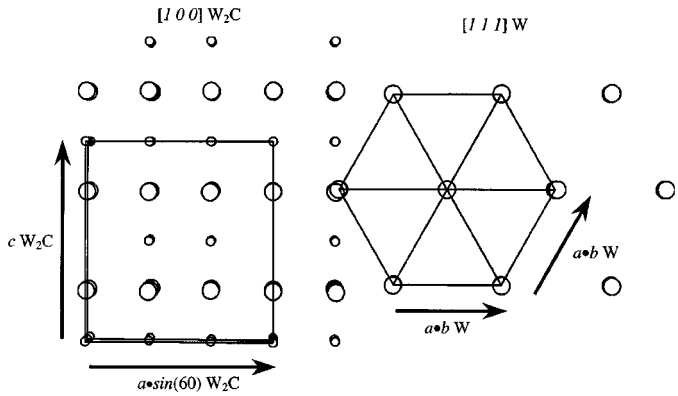

FIG. 8. [1 1 1] W and [1 0 0] W_2C projections (perpendicular to Fig. 7) showing the coherence in layer spacing between the two phases and the in in-plane displacements of W atoms relative to W_2C. The solid lines enclose one unit cell of each phase and W and C atoms are represented by large and small circles, respectively.

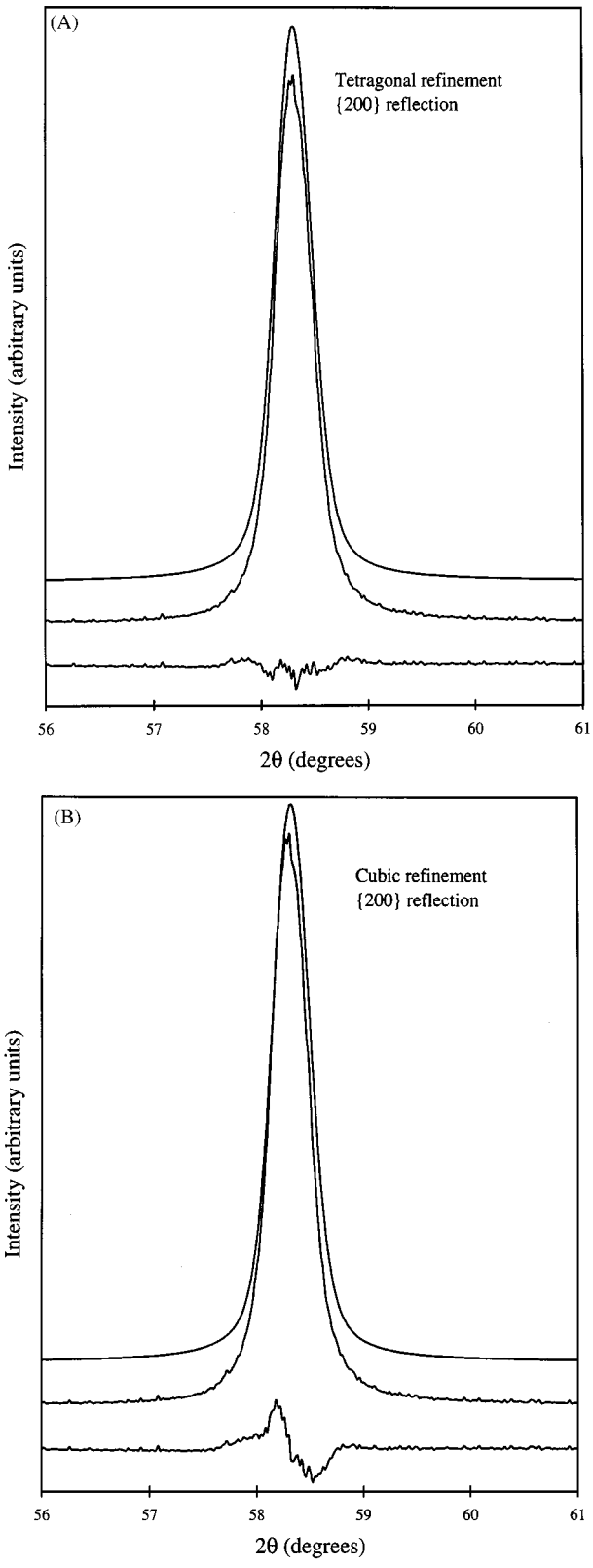

FIG. 9. Enlargement of the Rietveld profile fit of W milled for 10 min, highlighting the better fit to the tetragonal distortion (a) compared to the cubic lattice (b).

TABLE 15
Rietveld Refinement Parameters for TiC

Milling time	u	w	Lorentzian	TiC unit cell a (Å)	B_{iso} (Å^2)	Bragg R factor
33 min	0.009	− 0.005	0.231	4.329	0.1706	2.1

plane, forming laterally (i.e., parallel to (001) of host lattice) expanding islands of the oxide. Therefore, once each layer acquires some strain with the ingress of foreign atoms, a runaway reaction of layer inclusion ensues (32). The difference between this reaction mechanism and the previous one is apparent by comparison of Fig. 10 with Fig. 7. In W_2C formation, the carbon slips between layers of W atoms, whereas in TiC, each hexagonal layer itself must incorporate the carbon atoms.

The acquisition of anisotropic strain by titanium prior to reaction may be seen with careful analysis of peak shapes of diffraction from high-symmetry planes in samples milled for 30 min compared to the unmilled state (Fig. 10). (002) Bragg peaks from the milled specimen are sharper than (100) and (110) peaks. Furthermore, the basal reflections have a high angle "tail" characteristic of anisotropic smearing of the diffraction spots perpendicular to the scattering vector. In comparison, diffraction from the unmilled specimen shows good correspondence of individual peak widths with the bulk average, isotropic peak widths. Therefore, diffraction spots become flattened out in the $\{hk0\}$ reciprocal plane during milling. Physically, this phenomenon originates from loss of crystallographic order, or strain, preferentially in one direction. While the interlayer spacing of titanium is preserved, the structure within each basal plane becomes less well defined in the lead-up to reaction. These changes in crystallographic order over the course of the reaction are likewise reflected in the Ti ADPs, which decrease along $\langle 001 \rangle$ and increase along $\langle 100 \rangle$ and $\langle 110 \rangle$.

The cell dimension and diffraction peak shape of the TiC (Table 15) suggest that it is essentially stoichiometric, free of vacancies and free of crystallographic strain. Despite this, the TiC preserves some evidence of the reaction mechanism. Anisotropy of the $\{200\}$ and $\{220\}$ peaks (similar to that seen in the milled Ti) suggests layer disorder in the $\{111\}$ plane, which is perpendicular to both. This minor in-plane disorder is remanent from the layer slip required during formation.

CONCLUSIONS

The crystallographic pathways of the MA reactions $W + C \rightarrow WC$ and $Ti + C \rightarrow TiC$ were elucidated using

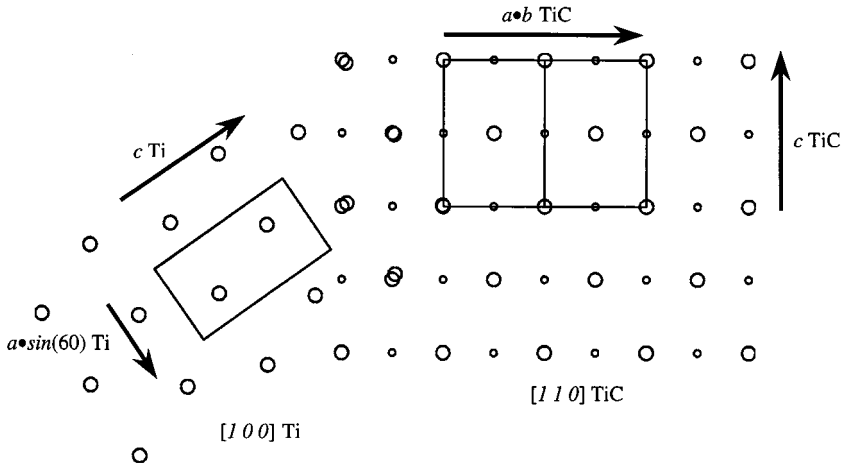

FIG. 10. Superposition of the TiC [1 1 0] and Ti [1 0 0] projections showing the metal planes in product and reactant are equally crowded, as opposed to the more open structure during W_2C formation (cf. Fig. 7). The Ti lattice loses coherence with the TiC lattice in this projection owing to the difference in layer stacking between the two lattices, (i.e., *ABABAS*-type vs *ABCABC*-type packing). The solid lines enclose one unit cell of each phase, and large and small circles represent Ti and C atoms, respectively.

Rietveld analysis of the diffraction data from intermediate stages in their production. These two reactions proceed through different pathways, which explains why W and C show a continuous reaction when mechanically alloyed, rather than the combustion reaction shown by Ti and C.

In the case of WC formation, as each reactant acquires strain, it proceeds to the next stable intermediate. It is shown that the required atomic displacements are unhindered and that a crystallographic relationship exists between the reactants and products at each of the stages in a continuous pathway. Rather than a discrete combustion event, the formation of the product therefore occurs over a period of time owing to the stability of the intermediates.

However, in the case of TiC formation, insertion of C into the Ti structure is associated with atomic rearrangements within crowded lattice planes. The energy requirements for transformation of Ti into TiC are therefore high. Once conditions are met for initial carbide formation, the entire Ti lattice is strained enough for a runaway reaction to occur and the material combusts.

ACKNOWLEDGMENTS

The authors thank Dr. Nick Kinaev for graphics assistance, and Lambert Bekessy for XRD support. This work was funded in part by the Australian Research Council.

REFERENCES

1. C. C. Koch, *Annu. Rev. Mater. Sci.* **19,** 121 (1989).
2. G. B. Schaffer and P. G. McCormick, *Mater. Forum* **16,** 91 (1992).
3. E. Bonetti, G. Scipione, G. Valdrè, S. Enzo, R. Frattini, and P. P. Macrì, *J. Mater. Sci.* **30,** 2220 (1995).
4. T. D. Shen, K. Y. Wang, J. T. Wang, and M. X. Quan, *Mater. Sci. Eng.* **A151,** 189 (1992).
5. H. Yang and P. McCormick, *J. Solid State Chem.* **19,** 258 (1993).
6. G. Le Caër, E. Bauer-Grosse, A. Pianelli, E. Bouzy, and P. Matteazzi, *J. Mater. Sci.* **25,** 4726 (1990).
7. A. H. Cottrell, *Mater. Sci. Technol.* **11,** 329 (1995).
8. J. S. Forrester and G. B. Schaffer, *Met. Trans. A* **26,** 725 (1995).
9. G. B. Schaffer and P. G. McCormick, *Met. Trans. A* **22,** 3019 (1991).
10. D. B. Wiles and R. A. Young, *J. Appl. Crystallogr.* **14,** 149 (1981).
11. C. J. Howard and R. J. Hill, Report No. M112, Australian Atomic Energy Commission, Sydney, Australia, 1986.
12. JCPDS—International Centre for Diffraction Data, 1996.
13. W. J. A. M. Peterse and J. H. Palm, *Acta Crystallogr.* **20,** 147 (1966).
14. J. C. Taylor, *Aust. J. Phys.* **38,** 519 (1985).
15. C. K. Johnson, "ORTEP: A FORTRAN Thermal-Ellipsoid Plot Program for Crystal Structure Illustrations," Report ORNL-3794, Oak Ridge National Laboratory. Oak Ridge, TN, 1965.
16. G. Caglioti, A. Paoletti, and F. P. Ricci, *Nucl. Instrum.* **3,** 223 (1958).
17. M. C. Favas, J. MacB. Harrowfield, D. L. Kepert, B. W. Skelton, L. M. Vitolo, and A. H. White, *Aust. J. Chem.* **45,** 1547 (1992).
18. N. J. Calos, J. S. Forrester, and G. B. Schaffer, *J. Solid State Chem.* **122,** 273 (1996).
19. G. M. Wang, S. J. Campbell, A. Calka, and W. A. Kaczmarek, *J. Mater. Sci.* **32,** 1461 (1997).
20. P. Haasen, "Physical Metallurgy," 2nd ed., p. 264. Cambridge Univ. Press, Cambridge, UK, 1986.
21. A. Hårsta, S. Rundqvist, and J. O. Thomas, *Acta. Chem. Scand. A* **32,** 891 (1978).
22. B. Lönnberg, T. Lundström, and R. Tellgren, *J. Less-Common Met.* **120,** 239–245 (1986).
23. L. N. Butorina and Z. G. Pinsker, *Soviet Phys. Crystallogr.* **5,** 560 (1960).
24. H. J. Goldschmidt, "Interstitial Alloys," p. 37. Butterworths, London, 1967.

25. H. J. Goldschmidt and J. A. Brand, *J. Less-Common Met.* **5,** 181 (1963).
26. O. N. Carlson, J. F. Smith, and R. H. Nafziger, *Met. Trans. A* **17,** 1647 (1986).
27. B. V. Khaenko, *Dopov. Akad. Nauk Ukr. RSR, Ser. A: Fiz. Mat. Tekh. Nauki* **42**(5), 85 (1980).
28. A. N. Christensen and B. Lebech, *Acta Crystallogr. B* **35,** 2677 (1979).
29. H. Hahn, *Z. Anorg. Chem.* **258,** 58 (1949).
30. E. H. Kisi, S. J. Kennedy, and C. J. Howard, *J. Am. Ceram. Soc.* **80,** 621 (1997).
31. K. J. Rawlings, S. D. Foulias, and B. J. Hopkins, *J. Phys. C: Solid State Phys.* **14,** 5411 (1981).
32. T. Matsuyama and A. Ignatiev, *Surf. Sci.* **102,** 18 (1981).
33. M. E. Bridge and R. M. Lambert, *Surf. Sci.* **82,** 413 (1979).
34. B. Klingenberg, F. Gellner, D. Borgmann, and G. Wedler, *Surf. Sci.* **296,** 374 (1993).